

# A combined experimental and simulation approach for short circuit prediction of 18650 lithium-ion battery under mechanical abuse conditions

Muhammad Sheikh<sup>a,\*</sup>, Ahmed Elmarakbi<sup>b</sup>, Sheikh Rehman<sup>c</sup>

<sup>a</sup> WMG, The University of Warwick, Coventry, CV4 7AL, United Kingdom

<sup>b</sup> Department of Mechanical and Construction Engineering, Faculty of Engineering and Environment, Northumbria University, Newcastle, NE18ST, United Kingdom

<sup>c</sup> University of Sunderland, Faculty of Technology, Sunderland, SR6 0DD, United Kingdom



## ARTICLE INFO

### Keywords:

Short circuit  
Cylindrical cells  
Concentric layers  
Numerical simulation  
Finite element analysis

## ABSTRACT

Lithium-ion batteries are considered an efficient energy source for current electric vehicles (EVs); however, the safety of these batteries is vital when it comes to large-scale deployment. Short circuit of batteries is one of the concerns as it can spread quickly within the battery module or pack if not controlled at the cell level. In this paper, single lithium-ion battery cell is investigated where mechanical abuse conditions are applied to investigate short circuits and propagation of failures due to short circuits. The numerical simulation tool LS-DYNA is used for the battery-layered model, each layer thickness is considered 0.3 mm, and concentrically layered formation is used for this purpose. An improved element size of 0.5 mm is used for steel casing and 1 mm for all other layers. A total of 27 layers are simulated in a single cell and the innermost radius is considered 1 mm. Displacement at short circuit, mean temperature at the short circuit, and mean maximum temperature change criterion are used to understand short circuit and propagation of failures. Simulation models are developed for quasi-static load analysis to understand the severity of failures, which can be used to reduce the risk of sequential failure of batteries in the battery pack.

## 1. Introduction

EV manufacturers have used various types of batteries for their fleets where the choice of battery depends on several aspects including power draw, capacity, thermal stability [1], and crash safety. Crash safety or crashworthiness of the lithium-ion battery is a crucial aspect as high battery content in EV battery packs poses some safety risks such as electricity damage, battery pressure, combustion, electrolyte splash, and heat damage. These failure scenarios can raise safety, durability, uniformity, and cost concerns and impose limitations on the wider applications of lithium-ion batteries in vehicles [2–5]. Due to the chemical properties of lithium-ion batteries, they can adapt higher temperatures quickly [6], and these higher temperatures can trigger exothermic chemical decomposition of lithium-ion battery component materials [7,8] that lead to further temperature rise and possibly catastrophic failure of the lithium-ion battery system [9] and permanent failure/thermal runaway. Temperature variations of lithium-ion batteries depend on the operating conditions. Under normal operating conditions temperatures of these batteries can be easily controlled to remain in the safe range, whereas stressful conditions such as high power draw at high ambient temperatures as well as defects in

individual cells may steeply increase local heat generation [8,10–19]. A few of the failure scenarios of lithium-ion batteries are:

- Overcharge of an individual cell or the entire battery pack
- Internal short circuit (ISC) of cells resulting due to an internal foreign object
- Crushing or penetration of a cell
- An external short circuit of a cell module or pack
- Exposure to abnormally high temperatures
- Fire or failure of neighbouring components

Lithium-ion cell thermal behavior for charge and discharge under normal conditions and possible thermal runaway was examined in [9] and [20–24]. It is also evident from [19] and [20] that external loading conditions including nail penetrations, mechanical abuse, and thermal abuse are commonly used abusive conditions for failure analysis. Jelllyroll failure is widely studied for battery failures but life prediction based on various abuse condition is not detailed and require both experimental and simulation approach to validate results. In some of the cases, signs of extreme mechanical conditions were found which are necessary to investigate the behavior of the cells following an impact,

\* Corresponding author.

E-mail address: [muhammad.sheikh@warwick.ac.uk](mailto:muhammad.sheikh@warwick.ac.uk) (M. Sheikh).

and would allow improvements to be made to the safety of the design of the vehicles and the batteries. Furthermore, this will allow a baseline for 'normal' thermal behavior to be developed supporting the detection of abnormal conditions [25,26].

To better understand battery properties due to abuse conditions, a model is required to represent battery operation, which also integrates electrical, thermal, and physical behavior due to mechanical abuse. Finite element methods are widely used to understand cell internal damage and the effect of damage conditions on adjacent components [2]. In this paper, the cylindrical lithium-ion cell is investigated using a finite element model (FEM) for its material properties and possible structural deformation.

Battery abuse testing, as detailed in [6,9], and [25–30] is used for safety analysis and prediction of failures. Lithium-ion 18650 cylindrical cell layer model has not been considered in detail and state of charge (SoC) induced changes are not found. The lack of research to investigate battery behavior in detail, as well as the role of testing batteries for early detection of short circuit for EV safety and stability has encouraged the investigation of this significant issue in detail. Failure of a lithium-ion battery can occur due to internal or external abuse conditions and triggers for external abuse conditions are crash/impact, charge/discharge discrepancies, and thermal abuse. Internal abusive conditions are considered to be internal short-circuit, excessive heating due to resistance build-up, and failure of internal battery components [31]. Different approaches are used to investigate short circuit of batteries where mechanical loading is used to perform abuse testing. Temperature variations are not considered in battery abuse failure, and is useful to predict battery degradation and short circuit; however sudden voltage drop due to applied force used as a failure of battery and initiation of the short circuit. Force-displacement, voltage-temperature and rate of temperature increase are used to study failure of lithium-ion battery, which lead to short circuit of individual cells.

## 2.1. Experimental study

Cells used for this study are Samsung 2200mAh lithium-ion cells from Samsung, Korea. The cell has dimensions of 18 mm diameter and 65 mm length with LiCoO<sub>2</sub>/graphite chemistry. Two sets of experiments are used, where the first experiment is used for cell conditioning using the charge, discharge, continuous monitoring of temperature and open-circuit voltages (OCV where voltage and temperature variations are important to understand short-circuit. In the second set of experiments, a controlled chamber is used to provide maximum protection to equipment and personnel. A calibrated mechanical press is used which

is equipped with a data logger, thermal camera, and laptop (PC) to capture and record data. The experimental setup is shown in Fig. 1.

In this paper, mechanical abuse conditions are comprised of quasi-static loading where four test protocols which are rod, circular punch, three-point bend, and flat plate are used for mechanical abuse conditions. The loading speed used is 1 mm/min. Trials were run in four different states of charge SoCs (0%, 25%, 50%, and 75%) with five repeated tests to evaluate short circuit [32].

## 2.2. Mechanical loading conditions

In this section first instances of short circuit with observed values are discussed where the initial and final time of observation and final voltages are detailed. This section serves the purpose of including detailed values in the form of a table where numeric values used in this section are useful to relate short circuit occurrence with other failures as mentioned throughout this section. Following nomenclatures are used for all test conditions and SoC is mentioned at the end with 0, 25, 50, and 75.

$t_{r,c,t,f}$  = time of short circuit occurrence

$F_{r,c,t,f}$  = applied force

$d_{sr,c,t,f}$  = displacement at short circuit

$T_{ir,c,t,f}$  = initial temperature before short circuit occurrence

$T_{fr,c,t,f}$  = final temperature

$\Delta T_{r,c,t,f}$  = change in temperature

$V_{i,r,c,t,f}$  = Initial Voltage

$\varepsilon_{nr,c,t,f}$  = nominal failure strain

$\sigma_{nr,c,t,f}$  = nominal failure stress

### 2.2.1. Rod test

A rod with diameter 11.70 mm and length 33.20 mm was used, which is 'T' shaped and the material used is alloy steel. A rigid base plate is placed beneath the cell, which is tightened from the bottom and fixed on a mechanical press.

The post-failure structural analysis is conducted to understand failure location with various SoC and loading conditions. Terminal shapes, crack locations, the formation of the crack, top, and bottom cell geometries are discussed in this section. As shown in Fig. 2(c), for rod tests due to load at the center location, cell deforms drastically, and buckling of layers occurred. Experimental result values are given in Table 1.

Force and SoC shows linear relationship where with lower SoC less force is applied but nominal strain values vary which is due to fluctuation in applied force. Voltage drop and temperature increase is also

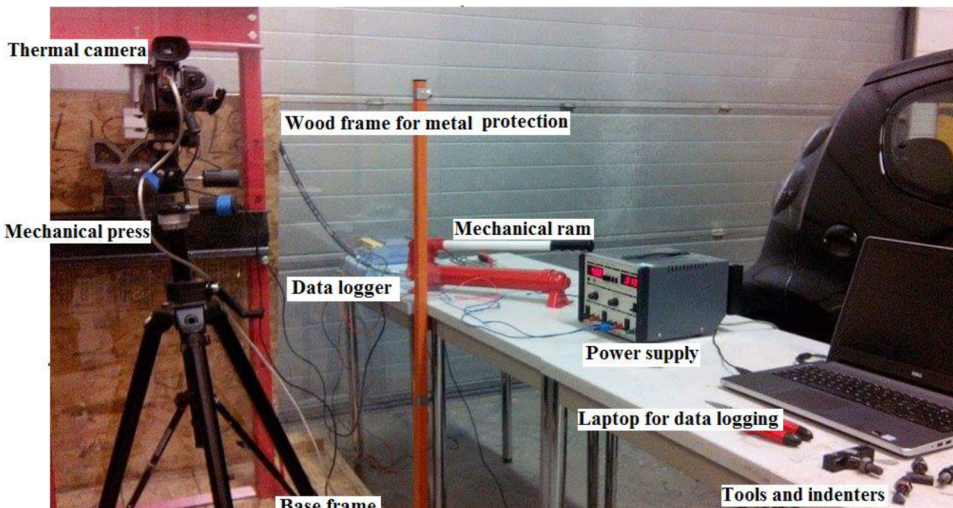
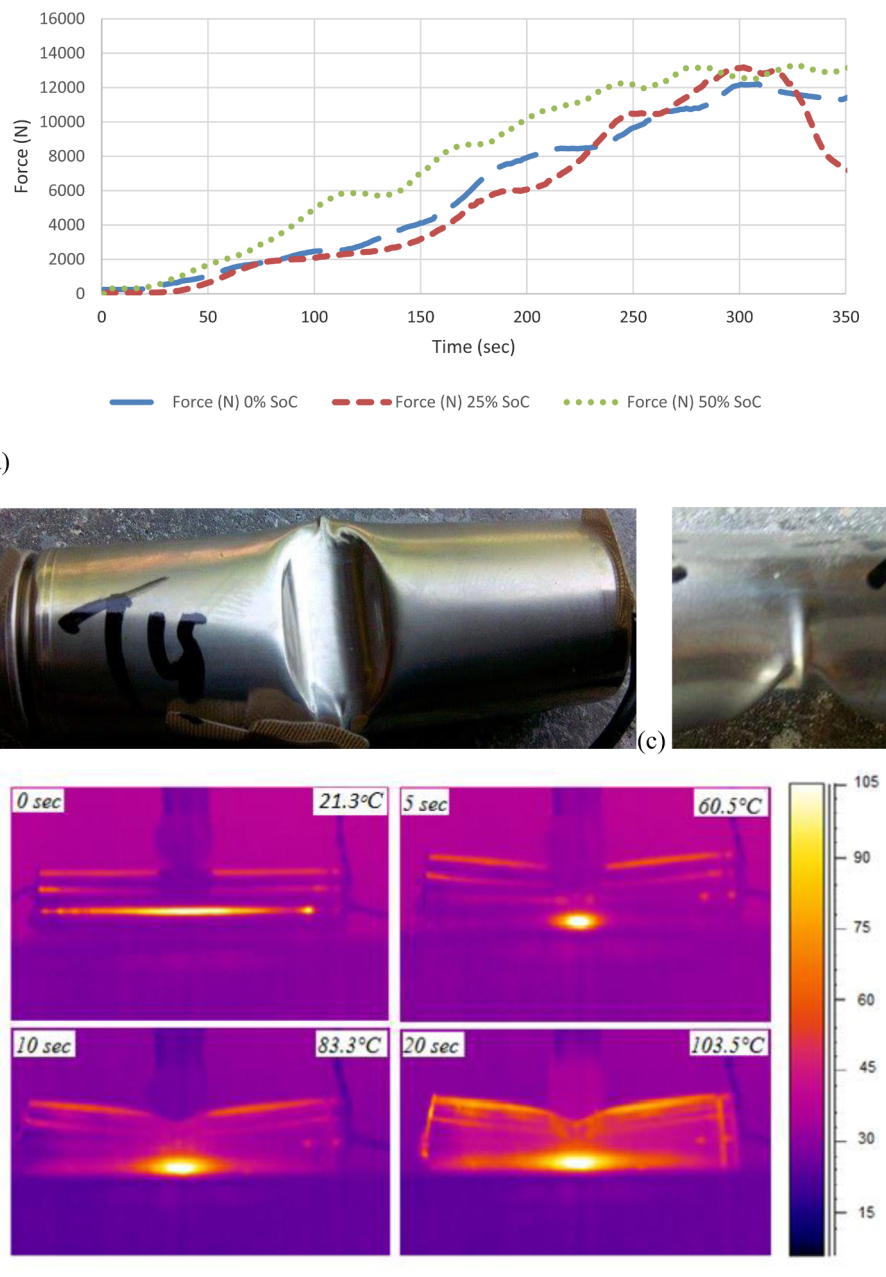


Fig. 1. Experimental setup for battery abuse testing.



**Fig. 2.** (a) Force and time relation, (b) Rod test cell deformation top view, (c) Cell deformation, buckling of top, (d) Sequential temperature variations for cell failure at 75% SoC rod test.

observed. It can be seen that the formation of crack did not occur in the rod test when the cell experienced a short circuit, however, immediate short circuit initiation and voltage drop without structural damage shows internal layer damage where current terminals are intact and no cell swelling, smoke or fire is observed. An almost similar pattern is observed at all SoCs for repeated tests, so cell labeling is not used. As shown in Fig. 2(c), the initial hotspot shows the highest temperature location is bottom mid surface but as time passes hotspot location changes and it moves to terminals (positive and negative terminals). Temperature variation is not uniform, and change in temperature location caused the dip in temperature values, which gets stable after this change. Change of temperature location shows the propagation of the damage in the internal electrochemistry and stiffnesses of individual layers, which change once cells experience thermal shock or excessive heat generation.

### 2.2.2. Circular punch

A circular punch with an outside diameter 15 mm, height 24.50 mm, and inside diameter 11.70 mm was designed with alloy steel material using the same safety precautions for testing as for rod test. A rigid flat plate was used for the base, which was fixed on a mechanical press. In the case of a circular punch test, slow build-up of temperature is observed, with no fracture, however, the deformation of steel casing, which also deforms internal layers, is observed.

In the circular punch test, no fracture is observed but a high buckling ratio compared to other tests was observed, which was mainly due to the shape of the indenter as shown in Fig. 3(c).

In a circular punch test, due to buckling, cell temperature and voltage change occurred sequentially but after removing force when the cell was left to observe temperature variations, it was found that the temperature change rate was very high in the circular punch test, which can be attributed to uneven buckling. As deflection was occurring, it

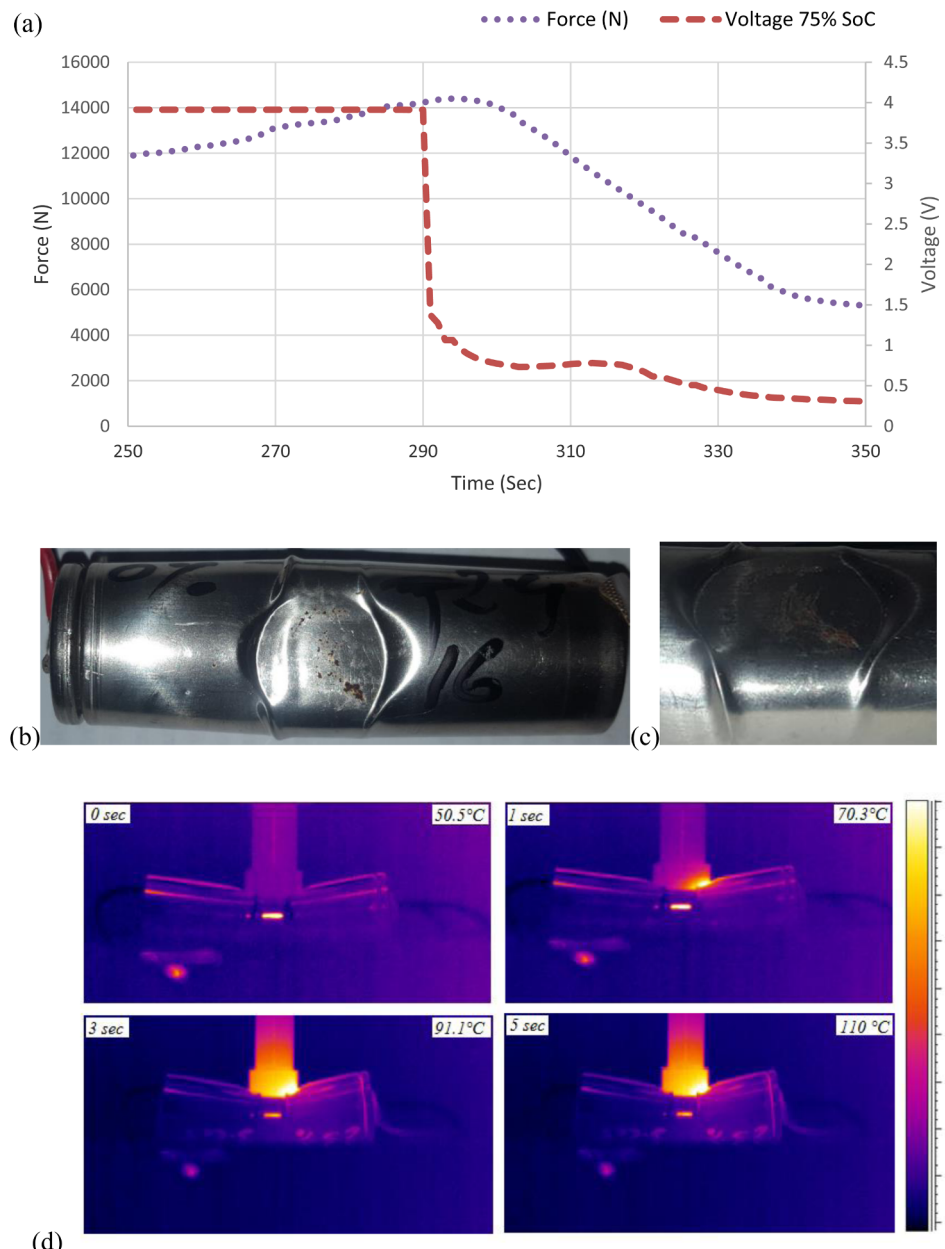


**Fig. 3.** Circular punch test, (a) force and voltage relation at 75% SOC (b) Cell deformation side view, (c) buckling at side, (d) temperature variations for circular punch test at 75% SoC.

means applied load did not affect the cell's load-carrying capability. Experiemental result values are given in Table 2.

As shown in Fig. 3(c), within 5 secs cells attained 60°C temperature. Change of temperature rate is higher, as at this ratio of temperature change, a cell can undergo burning within a minute and this change rate also affects the test impactor which lost its protective coating and started to work as the metal heat sink. As time progressed the cell dissipated heat to contact where contact temperature increase and cell temperatures at terminals started to decrease. This is due to the metal object, which acts as a heat sink and cools down the cell where low temperatures are observed, however short circuit occurrence is observed as voltage variations are immense.

#### 2.2.3. Three-point bend

Specific cell holder and sharp edge indenter were designed, where dimensions for cell holders were 88 mm length, 56 mm width, and cell holder cuts of 19.7 mm. Cell holder supports were welded to 4 mm

thick bottom rigid plate and the gap between both holder plates was 42 mm. The indenter has a cone shape with a length of 7.4 mm and a thickness of 1 mm, where the total length of the indenter was 24.50 mm and rod diameter of 11.70 mm. At force ( $F_t$ ) 2.33KN short circuit occurred in 0% SoC test, where the complete discharge of cells took 110 s. Short circuit displacement ( $d_{st}$ ) was 6.46 mm, and temperature change ( $\Delta T_s$ ) was 16.3 °C, values are given in Table 3.

In a three-point bend test, cell bending and rupture are observed where cell bend gradually but the formation of crack occurs where a sharp edge establishes contact with the cell, this is shown in Fig. 4. Both cell fracture and buckling take place in a three-point bend test where a sharp edge indenter is used. Cell terminals and end caps are intact in this testing; however, cell thinning took place at the center of the cell. In this test, the indenter traveled 40% of the original cell diameter where the mean displacement is 7.27 mm.

Sideway deflection can be observed in the three-point bend which is due to the triangle shape of the indenter tip. At cell failure, the fracture

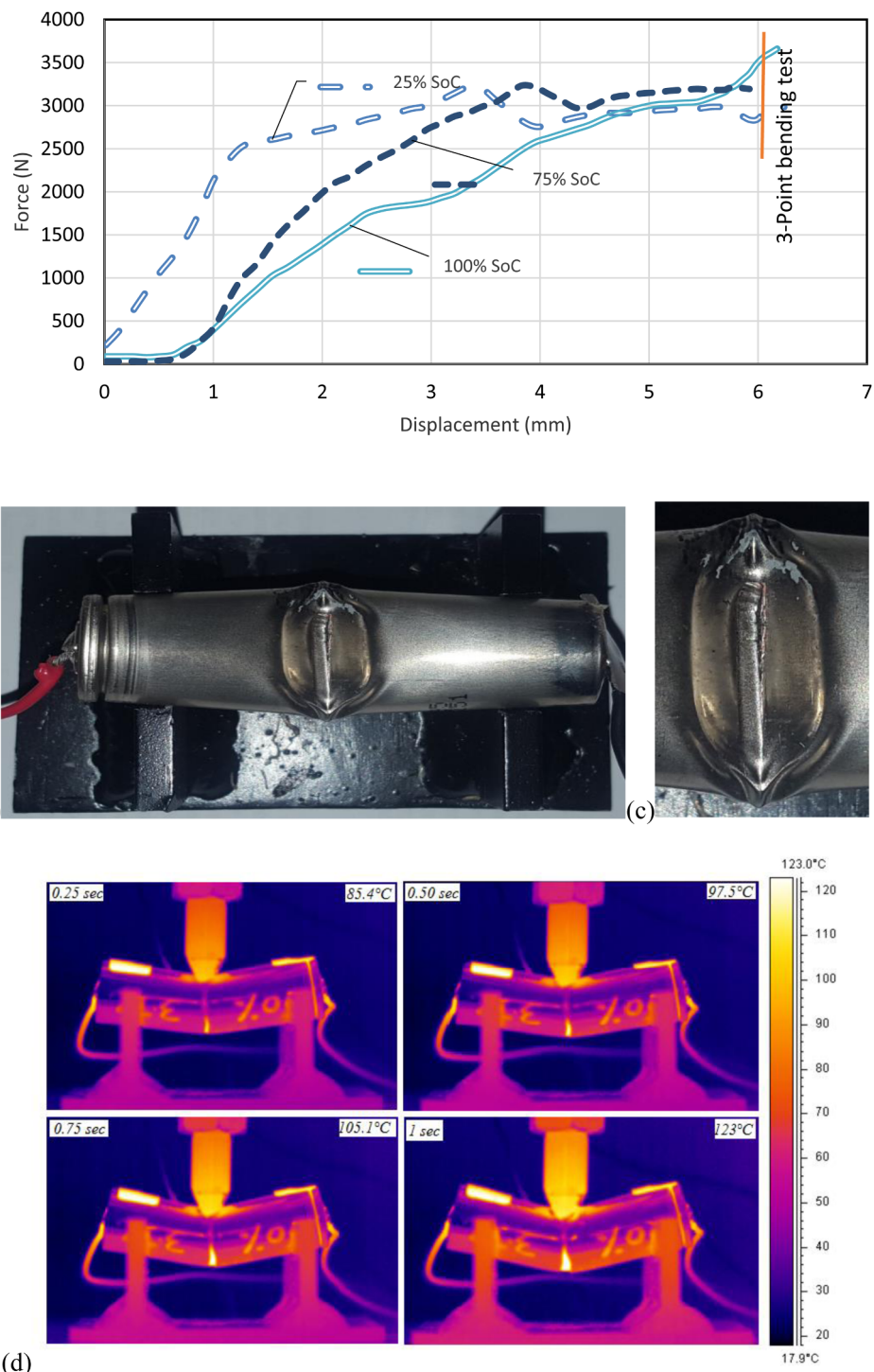


**Fig. 4.** Three-point bend test, (a) Force and displacement relation at different SoCs (b) Cell deformation top view, (c) Buckling and fracture of cell, (d) Initial results of temperature change for three-point bend test.

is observed in a three-point bend test where drastic temperature and voltage variations are observed.

For a three-point bend test, 75% SoC is chosen for further analysis where the high-temperature change ( $\Delta T_{75}$ ) and short circuit failure time ( $t_{75}$ ) is observed. In Fig. 4(c), hotspot development is very slow and spans the period, so sample time is not mentioned, which is discussed later. As shown hot spot location is the bottom of the cell where like circular punch after first loading indenter established contact with the cell casing and started to dissipate heat from the cell, so temperature change was observed for 1 s where the heat dissipation effect is

negligible. Unlike commonly reported bending and fracture patterns for a three-point bend test due to indenter shape cells showed fracture on the top surface and bending at the bottom.

#### 2.2.4. Flat plate deformation

A flat plate deformation test was conducted using a flat plate adaptor of length 70 mm and width 20 mm, which was fixed to load cell. The bottom plate was a rigid plate with much higher dimensions than the indenter and cell support was not used for this test. Test results obtained for flat plate deformation with a detailed parameter list, which

**Table 1**

Rod test results at short circuit development.

SoC	Time (Sec) <i>t<sub>r</sub></i>	Force (kN) <i>F<sub>r</sub></i>	Displacement (mm) <i>d<sub>sr</sub></i>	Initial temp (°C) <i>T<sub>ir</sub></i>	Final temp (°C) <i>T<sub>fr</sub></i>	Change in temp (°C) $\Delta T_r$	Voltage <i>Vi<sub>r</sub></i>	Nominal failure Strain <i>e<sub>nr</sub></i>	Nominal failure stress, $\sigma_{nr}$ (MPa)
0%	280	10.32	8.389	20.0	25.30	5.30	3.343	0.4661	8.754
25%	286	11.80	7.794	21.0	68.28	47.70	3.612	0.4160	10.419
50%	217	11.90	7.569	20.1	85.80	65.70	3.654	0.4205	10.676
75%	310	12.25	6.971	21.3	107.5	86.20	3.894	0.3870	11.490

**Table 2**

Circular punch compression test results at short circuit development.

SoC	Time (Sec) <i>t<sub>c</sub></i>	Force (kN) <i>F<sub>c</sub></i>	Displacement (mm) <i>d<sub>sc</sub></i>	Initial temp (°C) <i>T<sub>ic</sub></i>	Final temp (°C) <i>T<sub>fc</sub></i>	Change in temp $\Delta T_c$	Voltage <i>Vi<sub>c</sub></i>	Nominal failure Strain <i>e<sub>nc</sub></i>	Nominal failure stress, $\sigma_{nc}$ (MPa)
0%	420	9.56	5.431	19.2	35.6	16.4	3.325	0.301	10.241
25%	290	13.92	7.896	19.4	79.1	59.7	3.615	0.438	12.205
50%	454	13.20	7.459	19.8	99.9	80.1	3.697	0.414	11.936
75%	284	13.97	7.315	21.0	110.0	89.0	3.913	0.406	12.766

**Table 3**

Three-point bend test results at short circuit development.

SoC	Time (Sec) <i>t<sub>t</sub></i>	Force (kN) <i>F<sub>t</sub></i>	Displacement (mm) <i>d<sub>st</sub></i>	Initial temp (°C) <i>T<sub>it</sub></i>	Final temp (°C) <i>T<sub>ft</sub></i>	Change in temp $\Delta T_t$	Voltage <i>Vi<sub>t</sub></i>	Nominal failure Strain <i>e<sub>nt</sub></i>	Nominal failure stress, $\sigma_{nt}$ (MPa)
0%	390	2.33	6.46	20.9	37.2	16.3	3.310	0.344	2.276
25%	450	2.55	7.94	21.1	84.5	91.6	3.608	0.326	2.229
50%	465	2.57	8.40	23.1	114.7	63.4	3.663	0.321	2.184
75%	300	2.98	5.80	20.1	111.1	91.0	3.869	0.316	3.081

**Table 4**

Flat plate deformation test results at short circuit development.

SoC	Time (Sec) <i>t<sub>ff</sub></i>	Force (kN) <i>F<sub>f</sub></i>	Displacement (mm) <i>d<sub>sf</sub></i>	Initial temp (°C) <i>T<sub>if</sub></i>	Final temp (°C) <i>T<sub>ff</sub></i>	Change in temp $\Delta T_f$	Voltage <i>Vi<sub>f</sub></i>	Nominal failure Strain <i>e<sub>nf</sub></i>	Nominal failure stress, $\sigma_{nf}$ (MPa)
0%	790	42.0	5.548	20.0	117.9	97.90	3.546	0.308	44.490
25%	500	43.0	6.320	20.1	126.5	106.4	3.605	0.351	42.514
50%	195	41.6	6.367	20.3	150.3	130.0	3.714	0.350	40.958
75%	380	44.1	7.331	20.9	157.5	136.6	3.886	0.407	40.281

contributes towards short circuit, are given in [Table 4](#). Low short circuit displacement (*d<sub>sf</sub>*) compared to other test scenarios was observed in this test. High-temperature change ( $\Delta T_f$ ) was observed in all cases.

In flat plate deformation due to the large contact area of flat plate impactor, the cell attains an elliptical shape, where no fracture occurred; however, end caps removed from the terminal, which was due to high force impacts and the formation of end caps. Flat plate deformation is shown in [Fig. 5](#).

In [Fig. 5\(b\)](#) removal of the end cap at the positive terminal is highlighted, although there is a narrow gap, and the cell internal protection layer did not allow the cell to undergo smoke or fire but this indicates that damage to end caps can cause severe electrical and thermal changes. In this testing, however, the cell undergoes the complete change of shape from cylindrical to elliptical, which caused high-temperature increase as internal layers are very thin, and evolving shape might cause layers to develop the crack which created electrode contacts to initiate short circuit. Electron microscopy, computer tomography scan (CT scan), and X-ray scan are a few of the methods being used for cell post-failure analysis where internal damage behavior of layers is investigated. In flat plate deformation, the cell bears a significant amount of force before going into a short circuit state, once it went to short circuit temperature rise was very high.

Voltage drop as temperature increases is observed where at the high SoC, higher force and strain values are observed. Propagation of temperature change is shown in [Fig. 5\(c\)](#), where initial temperature contour with high-temperature variation was observed and very high

temperatures for the very short instant of time also observed. Once the cell attains peak temperature, then the negative terminal shows temperature which is due to the thermal conductivity of the negative terminal and internal failures, however; terminal wires are showing hotspot, no disconnection is noticed as voltage variations were observed throughout the test. Heat dissipation to surrounding and flat plate impactor was not observed which shows due to the even surface of the impactor, coating material did not come out which gave good results of temperature variations.

### 2.3. Summary of experimental results

Further analysis to understand the temperature effect at the occurrence of a short circuit is conducted and results are shown in [Fig. 6](#).

[Fig. 6](#), presents the mean maximum temperature for each loading condition by SOC. The temperature at short circuit occurrence has low values for low SOCs for all cells, and these values changed with the change in SOC. There is a positive trend where increases in SOC increase maximum temperature recorded at the point of the short circuit. The trends for three-point bend, rod, and circular punch tests are similar, but the trend for the flat plate is much steeper.

A model is fitted with the following formula to predict the maximum temperature of a cell following the short circuit in the flat plate test.

$$\ln(\text{Max Temp}) = 3.739 + (0.008 + 0.01982) \cdot \text{SOC} + (-0.056) \quad (1)$$

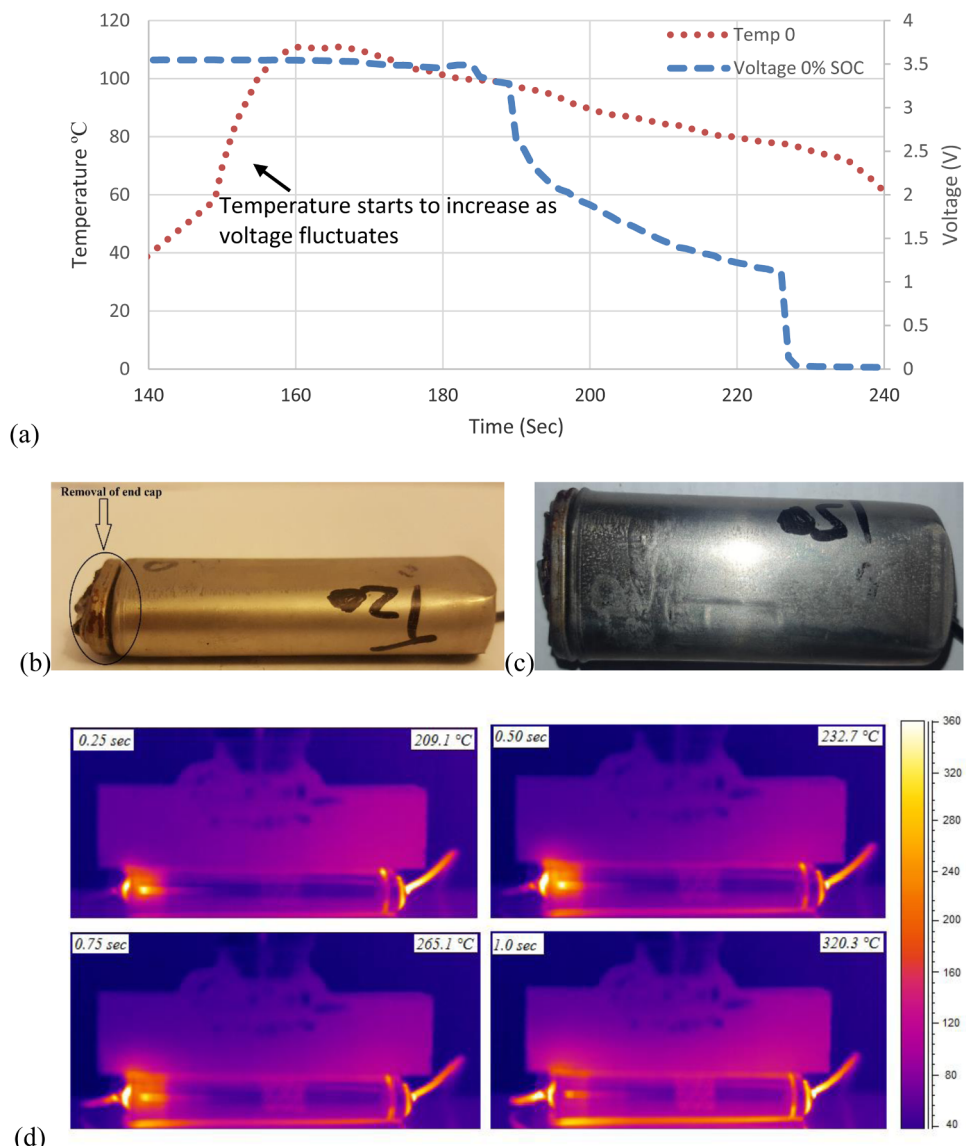


**Fig. 5.** Flat plate deformation, (a) temperature and voltage variations at short circuit, (b) removal of end cap, (c) top view of cell, (d) Propagation of short circuit with temperature for flat plate at 75% SoC.

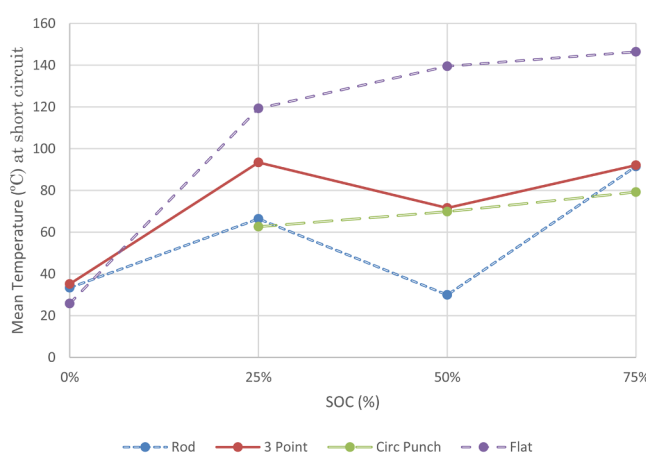


**Fig. 6.** SOC Vs mean peak temperature.

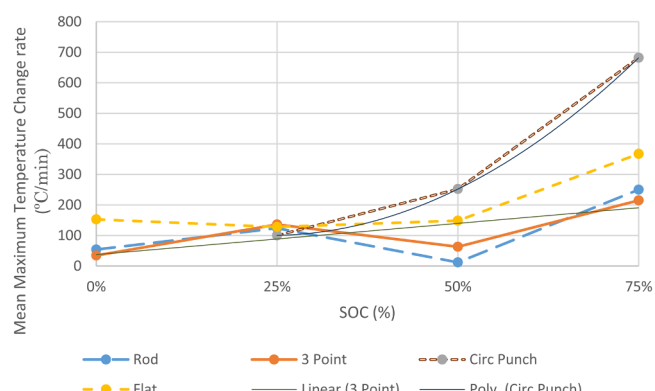


**Fig. 7.** Mean maximum temperature change rate for all tests.

Where Max Temp is the temperature in °C, SOC is the percentage state of charge out of 100.

The temperature change rate is the maximum change at the instant of short circuit which varies regardless of maximum temperature so that

**Table 5**  
LS-DYNA consistent units.

Consistent units								
Mass	Length	Time	Force	Stress	Energy	Density	Young's Modulus	
ton	mm	s	N	MPa	N-mm	(Tonne/mm <sup>3</sup> )	MPa	

temperature change rate is observed to explain the propagation of temperature change immediately after short circuit where the load is released and mean values are used for analysis as shown in Fig. 7.

SOC against mean peak temperature change (degrees/min) is presented in Fig. 7. Similar to above, it would appear there is generally a positive relationship between the rate of temperature change and SOC, but there seems to be less effect from test type, although circular punch is steeper than the other three test scenarios. Based on the previous analysis of displacement at short circuit, it can be concluded that it is likely that displacement has less effect on temperature if all conditions are not considered; therefore, models predict the temperature will include SOC and test type as predictor variables. Detail of all the values obtained is given in the next section with hotspot and local temperature change at the location of the short circuit.

A linear model predicting maximum temperature change is also used following the methods of the previous model. The final model for circular punch is:

$$\text{Max Temp Change} = 62.66 + (2.037 + 9.595)*\text{SOC} + (-299.46) \quad (2)$$

Where maximum temperature change is degrees/minute, C is 1 for circular punch loading conditions, and SOC is the state of charge out of

100. This model predicts the maximum temperature change concerning SOC.

### 3.1. Numerical simulation approach

Cell initial temperature is selected 22 °C, which agrees with single-cell testing standards and SAEJ2464 standard where 55 °C is recommended for module level test. The cell is modeled with fully integrated solid element formulation, where a total of 103,306 elements are used. The size of elements for steel casing is 0.5 mm and all other layers are 1 mm. The reason for different element size selection is to achieve accuracy, where steel housing is the first layer to experience load. All indenters and bottom plates are modeled as rigid geometry, where rigid material MAT\_20\_RIGID is used. The coefficient of friction between cells and support is 0.3 as given by [28]. No endcaps were considered for this simulation, however, SPC boundary conditions were used to restrain components of the battery if required. The failure strain of separator documented by [33] was 93%; however, the separator failure strain of 35% to 80% from literature is evident, which means values of 0.2 to 0.5 (50% or 80% of initial thickness) could be used for the separator. Consistent units by (LS-DYNA consistent units) were used for all simulation models and example units are given in Table 5.

The simulation model is designed to understand the loading impact on the cell and is based on the principles set in [30,31] and [34–36]. For simulation, all layers (steel shell casing, anode, cathode, separators, anode current collector, and cathode current collector) were 0.3 mm thick, and the innermost radius was 1 mm. Steel casing material is modeled using MAT-24-PIECEWISE-LINEAR-PLASTICITY in LS-DYNA.

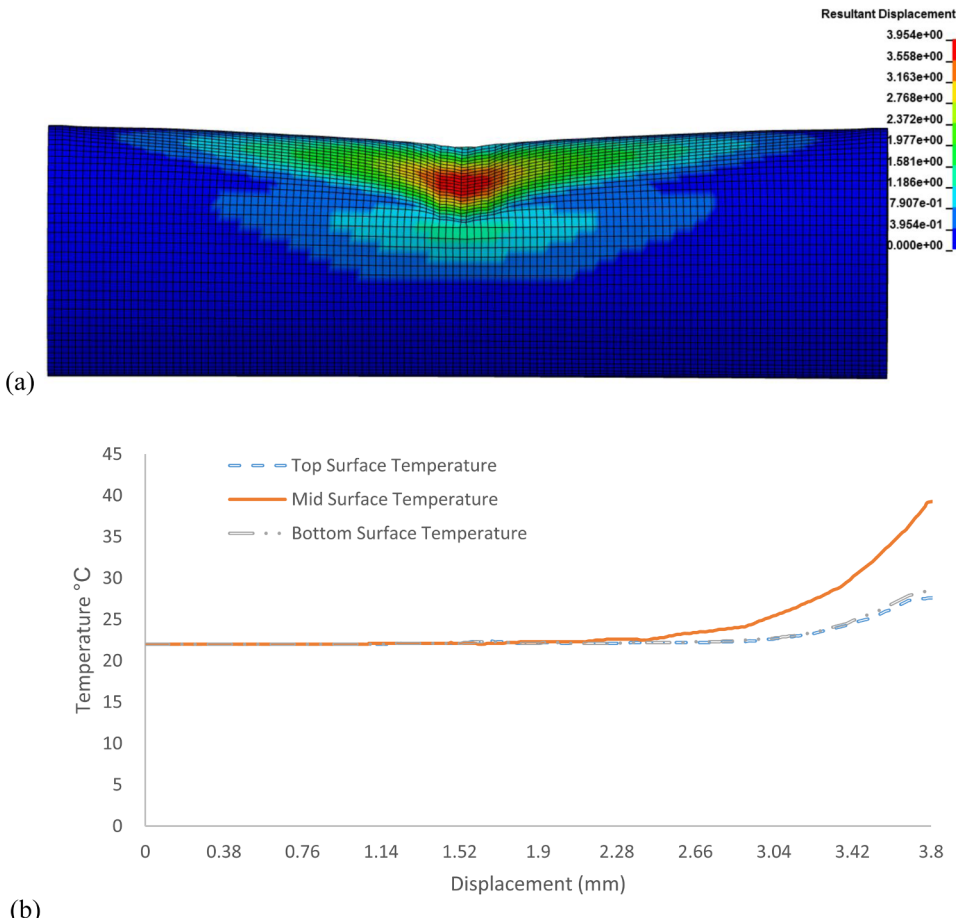


**Fig. 8.** Rod test (a) resultant displacement at initial failure, (b) Surface temperatures, quasi-static loading.

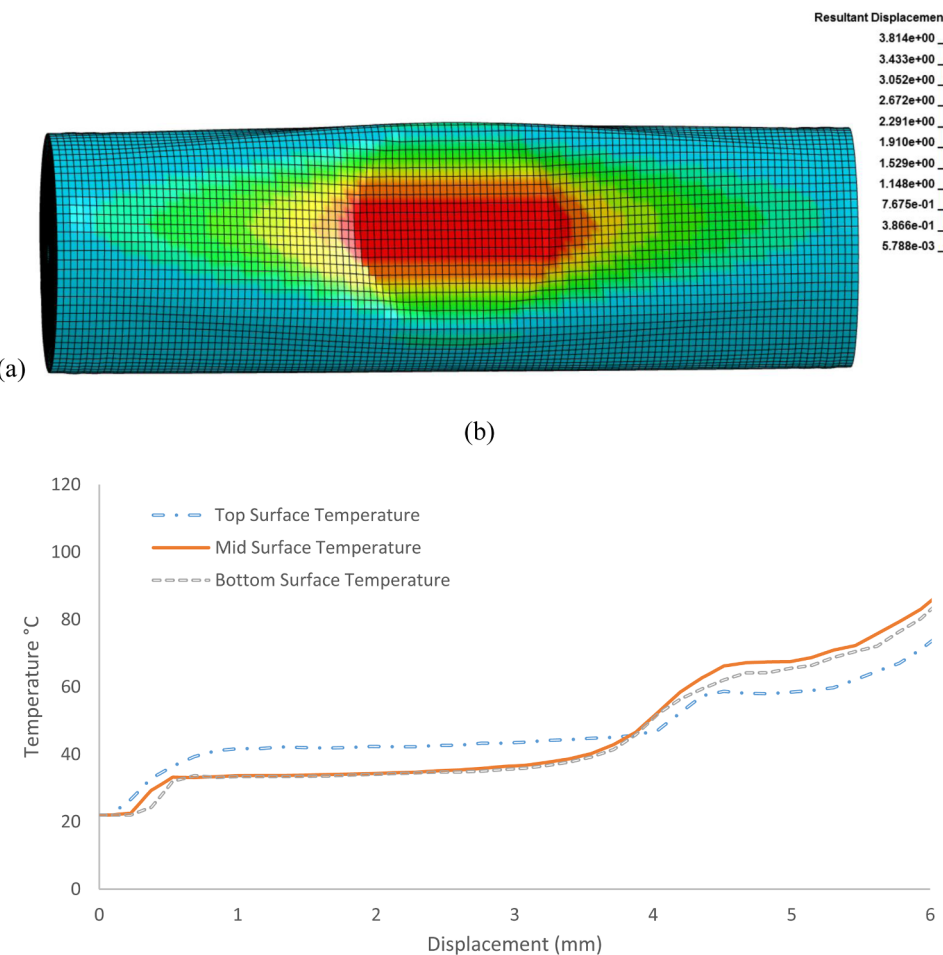


Fig. 9. Circular punch, (a) resultant displacement due to quasi-static load, (b) surface temperatures quasi-static load.

The separator, anode, and cathode were the MAT-63-CRUSHABLE-FOAM model, and anode current collector and cathode current collector were modeled using MAT-003-PLASTIC-KINEMATIC. The stress/strain curve for the separator, active anode material, and active cathode material was used from [37].

### 3.2. Simulation results and validation

Simulation models based on parameters and methods explained earlier are discussed in this section, where results for structural and thermal behavior and their comparison with experimental work are discussed. Quasi-static load simulation results are discussed in detail where displacement and temperature variations are discussed. Element erosion is used for fractures due to loading.

#### 3.2.1. Rod test simulation

Structural analysis was conducted and both experimental and simulation results matched for rod test simulation where, due to internal battery behavior, this response can vary for other tests. To negate the battery chemical proposition during loading, completely discharged cells are chosen to compare results, but in some cases, cell electrochemistry contributes towards cell stiffness, thermal variations, and short circuit response. In the simulation, a high-temperature change rate was observed at around 4 mm, which indicated the initiation of a short circuit or cell initial failure. Fig. 8, shows the simulation model of resultant displacement at the point of initial failure.

Temperature variation for quasi-static loading is discussed in detail where temperature and displacement relation shows the significance of temperature analysis for short circuit prediction.

Temperature cut-off was considered when a high-temperature change rate was observed, which indicated short circuit occurrence and temperature changes were considered at the point of force drop. Three surface locations were used to understand temperature behavior and results show temperature variations at the end terminals for quasi-static load are similar. In the experiment, the mid surface temperature at the point of the short circuit was 25 °C; however, results from quasi-static loading provided the closest value for simulation, which was 40 °C.

#### 3.2.2. Circular punch test simulation

Numerical simulation results showed similarity to the experiment result for structural deformation due to circular punch. In the numerical simulation analysis, the same deformation pattern as observed in experimental work was obtained where the size and location of deformation are the same. Punch shape stamped on the cell, where cell buckling is visible at the sides of the cell. The short circuit started to develop at 3.81 mm and short circuit displacement (dsc0) was found to be 5.6 mm, which is slightly higher compared to the experiment result. Fig. 9, shows resultant displacement at the initiation of a short circuit. Nominal failure stress for the experiment where a short circuit was initiated, was 10.24 MPa; however, in this simulation results showed stresses at the sides of the cell similar to rod test, which means even if the cell experiences high stress, failure of the cell depends on the

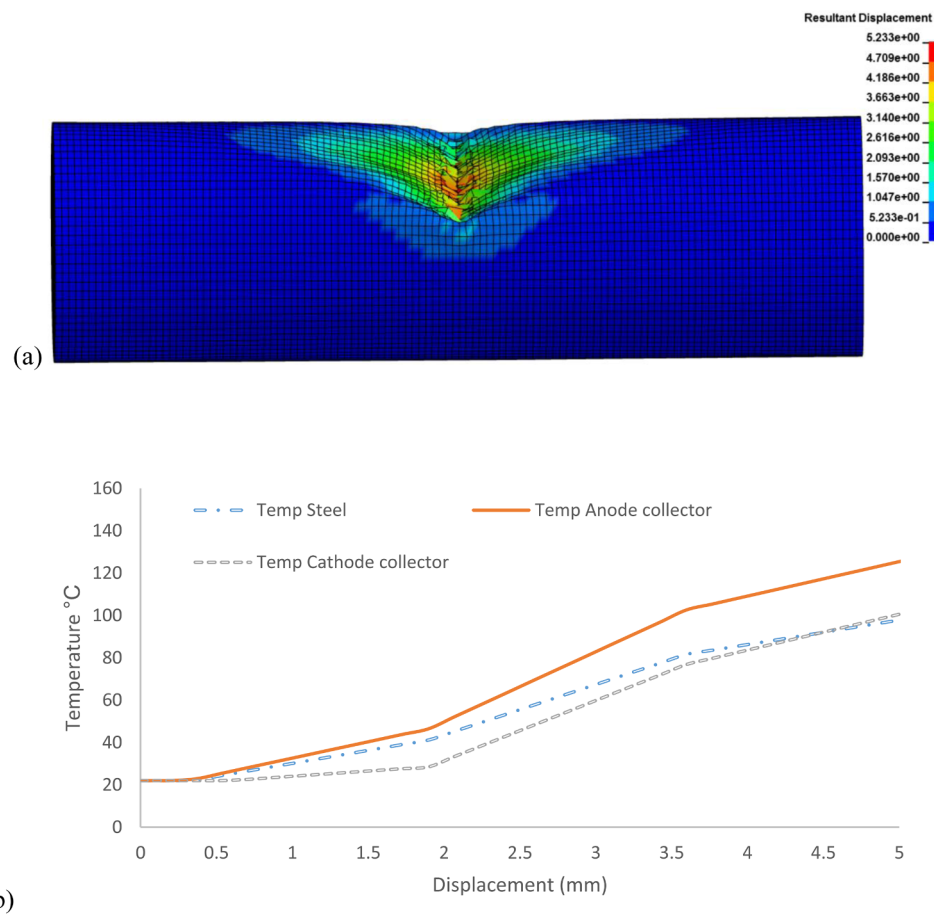


**Fig. 10.** Three-point bend test (a) Resultant displacement due to quasi-static load, (b) Temperature values for steel casing, anode current collector and cathode current collector.

location and speed of impact.

As shown in Fig. 9(b), the temperature at short circuit displacement for a mid surface with quasi-static load was 50 °C, and circular punch simulation results are close to experimental results when the quasi-static simulation is used, which allows layers to attain full mechanical strength and convert plastic work into heat accurately.

### 3.2.3. Three-point bend test simulation

For three-point bend test simulation, cell holders and sharp edge are modeled using rigid material. Due to computation efficiency, only modeled a sharp edge of the indenter and cell holders without supports. Boundary prescribed motion is used for indenter and SPC motion set was used for cell and base plates. Initially, when the load was applied on the cylindrical cell it used less force for compression but after some time due to material hardening excessive force was required for compression. Short circuit displacement was observed at 5.23 mm for quasi-static analysis. For quasi-static loading only steel casing experienced fracture but the temperature at other layers also increased at the time of short circuit which is explained in the following section. Fig. 10(a), shows resultant displacement due to quasi-static.

As can be seen from Fig. 10, sideways buckling of steel casing is found but due to sharp edge cell fracture is at the point of contact of a sharp edge. The cell experienced large deformation and fracture at the point of contact and layers were damaged. Temperature analysis due to quasi-static loading is discussed in the next section.

High temperatures after short circuit occurrence as shown in Fig. 10(b), are indicators of uncontrolled temperature, which can lead to further cell failures and can be resulted in a short circuit or thermal runaway. For a three-point bend simulation comparison of steel, anode

current collector and cathode current collector layers are used to understanding the temperature distribution of cells for internal layers, where anode current collector and cathode current collector indicate the first instance of short circuit. The temperature for steel and cathode current collector (aluminum) is around 100 °C; however, the temperature for anode current collector is around 130 °C at the time of short circuit occurrence.

### 3.2.4. Flat plate test simulation

Both experimental and simulation results showed identical deformation behavior for flat plate case. Cell layers ejection can be seen in the simulation model. In the experimental test, short circuit displacement (dsf0) was 5.5 mm and short circuit stress or tensile strength was 44.49 MPa; however, the force drops at 5 mm in this simulation model which indicates the short circuit. The deformed geometry model exhibits layers with dense displacement behavior in the area of the endcap, which shows high-stress values at that point as can be seen in Fig. 11.

For flat plate simulation, it is observed when the quasi-static load is applied, that cell temperature increased slowly during compression at the mid-surface, and maximum temperature was lower than the temperature observed during the experiment. Due to quasi-static loading, the cell exhibits a value around 120 °C at the time of short circuit displacement which is close to the value of the experiment work and validates experimental results for flat plate deformation at 0% SoC. Temperature variations for flat plate deformation vary at the top and bottom surfaces of the steel casing.

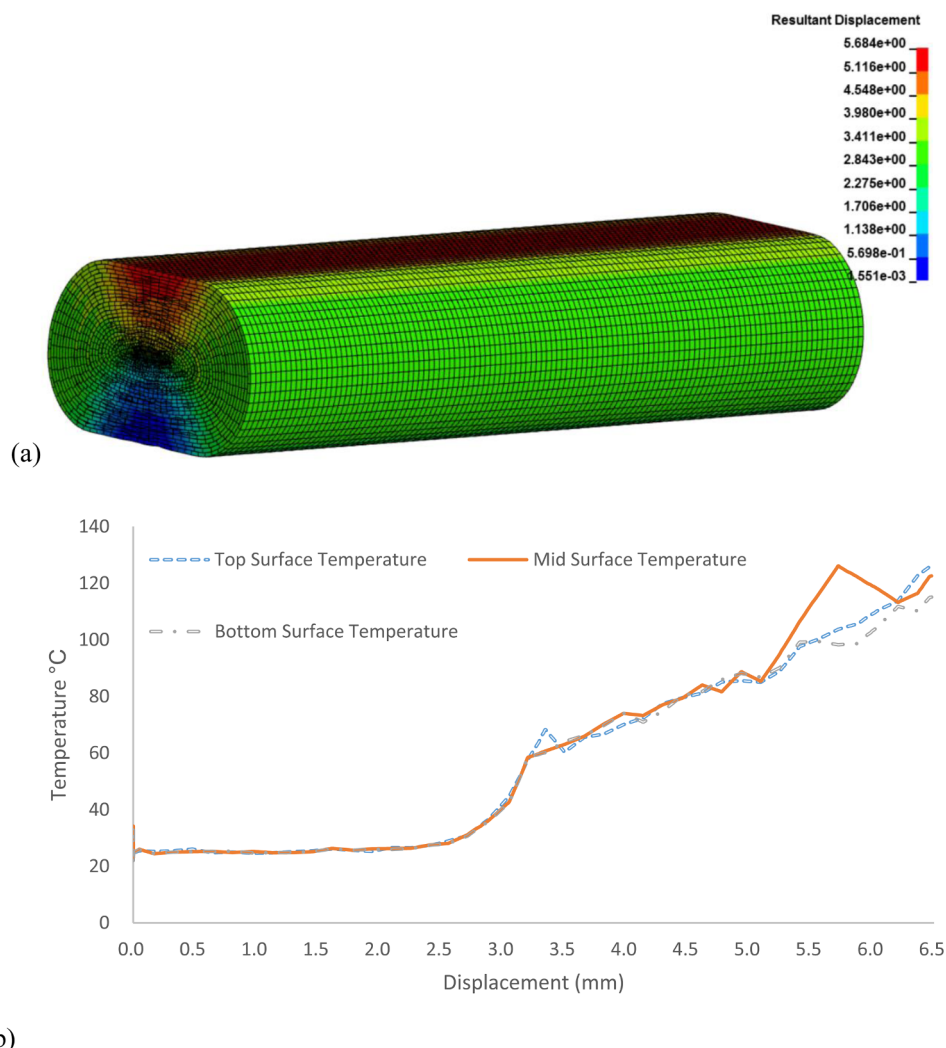


Fig. 11. (a) Resultant displacement for flat plate due to quasi-static load, (b) Flat plate surface temperature, quasi-static load.

#### 4. Conclusions

In this paper, battery failure analysis is carried out to predict short circuit, where the set of experiments are designed to conduct this analysis. Lack of research on SoC dependent failures of lithium-ion 18650 batteries provided the opportunity to investigate this in detail. Location and intensity of short circuit, time for the initial and complete failure of cells, and structural deformation are considered in detail, where modified test protocols are used. Temperature analysis using infrared cameras and thermocouples is used. Results obtained showed SoC dependency on failure pattern, wherewith different test protocols this dependency varies. Many indicators for the occurrence of cell failures are observed which are, force drop at the time of short circuit, temperature increase, temperature change rate, displacement, and sudden voltage drop. Sequential failures of battery following the short circuit are observed, where high-temperature variations were observed for the test with high SoCs. Due to a sharp edge, a three-point bend caused a fracture of the cell.

As evident from the results shown, the simulation model is capable of capturing cell mechanical and thermal responses, where cell electrochemistry and endcaps were not considered. Results obtained from simulation models correlated with experimental tests and significant improvement are observed including layer formations and short circuit failure criteria.

A comparison of experimental and simulation results is used to

understand sequential failures of battery structure and temperature variations, where it is evident from simulation results that quasi-static loading is suitable to predict short circuit and possible thermal runaway. For further work, this simulation model can be used for the analysis of the structural and thermal behavior of 18650 cells where electrochemistry of cells can be used to improve these results and failure predictions.

#### Authorship contributions

**Conception and design of study:** M. Sheikh, A. Elmarakbi;  
**Acquisition of data:** M. Sheikh  
**Analysis and/or interpretation of data:** M. Sheikh, Sheikh Rehman;  
**Drafting the manuscript:** M. Sheikh, A. Elmarakbi, S. Rehman;  
**Revising the manuscript critically for important intellectual content:** M. Sheikh, A. Elmarakbi, S. Rehman;  
**Approval of the version of the manuscript to be published:** M. Sheikh, A. Elmarakbi, S. Rehman;

#### Declaration of Competing Interest

This is to confirm that this work has not been submitted previously to the Journal of Energy Storage and it has not been published previously (except academic thesis), and is not submitted for publication

elsewhere, and is approved by all authors mentioned in the author list. All authors have participated in (a) conception and design, or analysis and interpretation of the data; (b) drafting the article or revising it critically for important intellectual content; and (c) approval of the final version. The authors have no affiliation with any organization with a direct or indirect financial interest in the subject matter discussed in the manuscript

## References

- [1] He H., Xiong R., Guo H., Li S., Comparison study on the battery models used for energy management of batteries in electric vehicles, *Energy Convers. Manag.* (2012) 113–121.
- [2] Liu Y., Jia C., Yuan L., Wang X., Gao S., Yin J., Xu J., Safety issues and mechanisms of lithium-ion battery cell upon mechanical abusive loading: a review, *Energy Storage Mater.* 24 (2020) 85–112.
- [3] Zhang G., Cao L., Ge S., Wang C.Y., Shaffer C.E., Rahn D.C., In situ measurement of radial temperature distributions in cylindrical li-ion cells, *J. Electrochem. Soc.* 161 (10) (2014) A1499–A1507.
- [4] Lisbona D., Snee T., A review of hazards associated with primary lithium and lithium-ion batteries, *J. Process Safety Environ. Protect.* 89 (2011) 434–442.
- [5] Kizilel R., Sabbah R., Selman J.R., Al-Hallaj S., An alternative cooling system to enhance the safety of li-ion battery packs, *J. Power Sources* 194 (2009) 1105–1112.
- [6] Shi Y., Noelle D.J., Wang M., Le A.V., Yoon H., Zhang M., Meng Y., Qiao Y., Exothermic behaviors of mechanically abused lithium-ion batteries with Dibenzylamine, *J. Power Sources* 326 (2016) 514–521.
- [7] Wang L., Yin Z., Yu Y., Wang T.X., Yu J., Zhao Z., Xie Y., Li J., Xu J., Unlocking the significant role of shell material for lithium-ion battery safety, *Mater. Des.* 160 (2018) 601–610.
- [8] Kim G.-H., Pesaran A., Spotniz R., A three dimensional thermal abuse model for lithium-ion cells, *J. Power Sources* (2007) 476–489.
- [9] Lopez C., Jeevarajan J., Mukherjee P., Characterization of lithium-ion battery thermal abuse behavior using experimental and computational analysis, *J. Electrochem. Soc.* 162 (10) (2015) A2163–A2173.
- [10] Liu J., Wang Z., Gong J., Liu K., Wang H., Guo L., Experimental study of thermal runaway process of 18650 lithium-ion battery, *Mater. (Basel)* 10 (3) (2017) 230.
- [11] S.J. Bazinski, Wang X., Experimental study on the influence of temperature and state-of-charge on the thermophysical properties of an LFP pouch cell, *J. Power Sources* 293 (2015) 283–291.
- [12] N.S. Spinner, R. Mazurick, A. Brandon, S.L. Rose-Pehrsson, S.G. Tuttle, Analytical, numerical and experimental determination of thermophysical properties of commercial 18650 LiCoO<sub>2</sub> lithium-ion battery, *J. Electrochem. Soc.* 162 (14) (2015) A2789–A2795.
- [13] L. Siguang, Z. Chengning, Study on battery management system and lithium-ion battery, *Proceedings of IEEE, International Conference on Computer and Automation Engineering (ICCAE 2009)*, 8–10, March 2009 Bangkok, Thailand.
- [14] R.R. Richardson, P.T. Ireland, D.A. Howey, Battery internal temperature estimation by combined impedance and surface temperature measurement, *J. Power Sources* 265 (2014) 254–261.
- [15] Y. Chen, J.W. Evans, Thermal analysis of Lithium-Ion batteries, *J. Electrochem. Soc.* 143 (1996) 2708–2712.
- [16] K. Smith, G.H. Kim, E. Darcy, A. Pesaran, Thermal/electrical modeling for abuse-tolerant design of lithium ion modules, *Int. J. Energy Res.* 34 (2) (2010) 204–215.
- [17] Y. Jia, S. Yin, B. Liu, H. Zhao, H. Yu, J. Li, J. Xu, Unlocking the coupling mechanical-electrochemical behavior of lithium-ion battery upon dynamic mechanical loading, *Energy* 166 (2019) 951–960.
- [18] S. Santhanagopalan, P. Ramadas, J. Zhang, Analysis of internal short-circuit in a lithium ion cell, *J. Power Sources* 194 (2009) 550–557.
- [19] R. Spotnitz, J. Franklin, Abuse behavior of high-power lithium-ion cells, *J. Power Sources* 113 (2003) 81–100.
- [20] S. Kalnaus, Y. Wang, J. Turner, Mechanical behavior and failure mechanisms of li-ion battery separators, *J. Power Sources* 348 (2017) 255–263.
- [21] G.H. Kim, K. Smith, J. Ireland, A. Pesaran, Fail-safe design for large capacity li-thium-ion battery systems, *J. Power Sources* 210 (2012) 243–253.
- [22] N. Lotfi, P. Fajri, S. Novosad, J. Savage, R.G. Landers, M. Ferdowsi, Development of an experimental testbed for research in lithium-ion battery management systems, *Energies* 6 (2013) 5231–5258.
- [23] D. Xu, L. Wang, J. Yang, Research on li-ion battery management system, *Proceedings of the International Conference on Electrical and Control Engineering (ICECE)*, 25–27, 2010 Wuhan, China.
- [24] D. Doughty, E.P. Roth, A general discussion of li-ion battery safety, *Electrochim. Soc. Interface (summer)* (2012) 37–44.
- [25] H. Yang, H. Bang, K. Amine, J. Prakash, Investigations of the exothermic reactions of natural graphite anode for li-ion batteries during thermal runaway, *J. Electrochem. Soc.* 152 (1) (2005) A73–A79.
- [26] Liu Y., Jia C., Li S., Yin C., Yuan Z., Hu L., Wang Y., Li J., Xu J., Safety issues caused by internal short circuits in lithium-ion batteries, *J. Mater. Chem. A* (2018) issue 43.
- [27] Wang L., Yin S., Zhang C., Huan Y., Xu J., Mechanical characterization and modeling for anodes and cathodes in lithium-ion batteries, *J. Power Sources* 392 (2018) 265–273.
- [28] Zhang Z., Jin P., Wyatt, "Electrochemical modeling of lithium plating of lithium ion battery for hybrid application", *SAE Int. J. Alternat. Powertrains* 6 (2017) 2.
- [29] J. Lamb, C. Orendorff, Evaluation of mechanical abuse techniques in lithium ion batteries, *J. Power Sources* 247 (2014) 189–196.
- [30] C.H. Yuan, X. Gao, H.K. Wong, B. Feng, J. Xu, "A multiphysics computational framework for cylindrical battery behavior upon mechanical loading based on LS-DYNA, *J. Electrochem. Soc.* 166 (6) (2019) A1160.
- [31] E. Sahraei, R. Hill, T. Wierzbicki, Calibration and finite element simulation of pouch lithium-ion batteries for mechanical integrity, *J. Power Sources* 201 (2012) 307–321.
- [32] M. Sheikh, A. Elmarakbi, M. Elkady, "Thermal runaway detection of cylindrical 18650 lithium-ion battery under quasi-static loading conditions, *J. Power Sources* 370 (2017) 61–70.
- [33] C. Zhang, S. Santhanagopalan, M.A. Sprague, A.A. Pesaran, Coupled mechanical-electrical-thermal modeling for short-circuit prediction in a lithium-ion cell under mechanical abuse, *J. Power Sources* 290 (2015) 102–113.
- [34] M. Sheikh, A. Elmarakbi, M. Elkady, Thermal runaway detection of cylindrical 18650 lithium-ion battery under quasi-static loading conditions, *J. Power Sources* 370 (2017) 61–70.
- [35] Wang L., Yin S., Xu J., A detailed computational model for cylindrical lithium-ion batteries under mechanical loading: from cell deformation to short-circuit onset, *J. Power Sources* 413 (2019) 284–292.
- [36] C. Yuan, X. Gao, H.-K. Wong, B. Feng, J. Xu, A multiphysics computational framework for cylindrical battery behavior upon mechanical loading based on LS-DYNA, *J. Electrochem. Soc.* 166 (number 6) (2019).
- [37] C. Zhang, S. Santhanagopalan, M.A. Sprague, A.A. Pesaran, A representative-sandwich model for simultaneously coupled mechanical-electrical-thermal simulation of a lithium-ion cell under quasi-static indentation tests, *J. Power Sources* 298 (2015) 309–321.